Chirality-Dependent Transport in Double-Walled Carbon Nanotube Assemblies: The Role of Inner Tubes

Kazunori Fujisawa,[†] Keita Komiyama,[†] Hiroyuki Muramatsu,[‡] Daisuke Shimamoto,[‡] Tomohiro Tojo,[†] Yoong Ahm Kim,[†,*] Takuya Hayashi,[†] Morinobu Endo,[†,‡] Kyoichi Oshida,[§] Mauricio Terrones,[⊥] and Mildred S. Dresselhaus[¶]

[†]Faculty of Engineering and [‡]Institute of Carbon Science and Technology, Shinshu University, 4-17-1 Wakasato, Nagano-shi, Japan, [§]Nagano National College of Technology, 716 Tokuma, Nagano 381-8550, Japan, [⊥]Department of Physics, Department of Materials Science and Engineering & Materials Research Institute, The Pennsylvania State University, 104 Davey Lab., University Park, Pennsylvania 16802-6300, United States, and [¶]Department of Electrical Engineering and Computer Science and Department of Physics, Massachusetts Institute of Technology, Cambridge, Massachusetts 02139-4307, United States

ABSTRACT A fundamental understanding of the electrical properties of carbon nanotubes is vital when fabricating high-performance polymeric composites as well as transparent conductive films. Herein, the chirality-dependent transport mechanisms in peapod- and chemical vapor deposition-grown double-walled carbon nanotubes (DWNTs) films are discussed by identifying the chiralities of the inner and the outer tubes using fast Fourier transform image processing, as well as optical studies (*e.g.*, Raman, UV, and photoluminescence spectroscopies). The observed conduction mechanisms are strongly dependent on the total fraction of the metallic inner and outer tubes within the DWNT samples. Furthermore, the contribution of the inner tubes to the electronic transport properties of DWNT films is confirmed by photochemically deactivating the outer tubes in both types of DWNT samples.

KEYWORDS: double-walled carbon nanotubes · buckypaper · conduction mechanism · chirality · fast Fourier transform

Carbon nanotubes (CNTs) consist of rolled graphene cylinders of nanometer size in diameter. Since a hexagonal sp^2 hybridized carbon layer exhibits a high mechanical strength, CNTs reveal excellent mechanical and electrical properties as well as flexibility. From these characteristics, CNTs are being considered as a multifunctional filler in the fabrication of composites and alternative transparent conductive films, able to replace indium tin oxide (ITO) in electronic displays.[1] When dealing with single-walled carbon nanotubes (SWNTs), their electrical properties are strongly dependent on the way the graphene sheet is rolled up to form a carbon cylinder. In theory, one-third of the SWNTs are metallic (including semimetallic) and the other two-thirds of SWNTs are semiconducting.[2] Recently, the chirality-dependent electrical transport properties of semiconducting and metallic SWNT films that were prepared using density gradient ultracentrifugation were well studied.[3] However, there are only limited studies available on the electric conductivity of multiwalled carbon nanotube (MWNT) films, since MWNTs possess many structural and morphological parameters such as length, diameter, number of the layers, and chiralities. In this study, we have selected double-walled carbon nanotubes (DWNTs) as the simplest model system for studying MWNT properties.[4] Geometrically, DWNTs consist of two coaxial SWNTs. Thus, the versatile outer tube chemistry and the protected electrical and structural properties of the inner tubes[5−7] make DWNTs potentially useful in the fabrication of field effect transistors,[8−10] stable field emitters,[11] electrode materials for storing lithium ions,[12] supporting materials for catalysts,[13] fillers in polymer composites, and biomarkers in the biomedical area.[14,15] In addition, sorted DWNTs with metallic outer tubes were demonstrated to be suited for use in transparent conductive film applications,[16] where electrical conductance, optical transparency, and mechanical strength are needed simultaneously because DWNTs are more resistant than SWNTs to the hydrodynamic shear forces generated by ultrasonication processes.[17] To date, DWNTs have been produced by several methods, such as arc discharge,[18−22] chemical vapor deposition (CVD),[23−25] and coalescence of peapods (C_{60}, C_{70} and ferrocene encapsulated inside SWNTs).[26−31] Peapods with the structure of SWNTs encapsulating C_{60} molecules are one example of a hybridized carbon nanomaterial. Since the first observation of the peapod morphology became available,[26] some groups

* Address correspondence to yak@endomoribu.shinshu-u.ac.jp.

Received for review July 8, 2011 and accepted August 12, 2011.

Published online August 12, 2011
10.1021/nn202541c

reported the coalescence of fullerenes inside SWNTs, and the subsequent formation of DWNTs under electron beam irradiation[27] or by thermal treatment in vacuum.[30] The photoluminescence (PL) signals from the semiconducting inner tubes of peapod-grown DWNTs were observed from DWNT samples that were prepared by thermally treating peapods above 1700 °C in argon using a graphite furnace.[32] However, even with the availability of high-purity DWNTs, there is still no systematic study on the electrical properties of pure and crystalline DWNT networks or films.

The purpose of this study is to understand the chirality-dependent conduction mechanisms of DWNT films using two different types of materials (*i.e.*, CVD-DWNTs[23] and peapod-DWNTs[32]). To identify the chirality distributions of the inner and the outer tubes of the peapod- and CVD-DWNTs, we have used a fast Fourier transform (FFT) image processing method based on atomic resolution TEM images, and we then compared the results obtained from their two-dimensional PL maps. Experimentally, we have confirmed the strong chirality-dependence of the conduction mechanisms and the contribution of the inner tubes to the bulk electronic transport in DWNT films, by deactivating the sidewall of the outermost tubes with covalently anchored functional groups using a photochemical treatment.

RESULTS AND DISCUSSION

To prepare DWNT film, CVD- and peapod-DWNT samples (15 mg) were dispersed in ethanol (100 mL) using ultrasonication (Kubota UP50H) for 30 min without any surfactant. By filtering a stable suspension of DWNTs (polytetrafluoroethylene filter, 1 μm) and drying it for 24 h in vacuum, we have prepared a thin but round DWNT film by peeling off the film from the filter (Figure 1a).[33] Easy fabrication of such a strong, flexible DWNT film comes from the strong physical entanglement of the long bundled DWNTs (Figure 1b). In addition, we have carried out a detailed TEM observation in order to examine the geometry and the crystallinity of SWNTs, peapods, CVD- and peapod-DWNTs used in this study. The long and crystalline SWNT with a diameter of 1.3 nm exhibits a hexagonal Moiré pattern (Figure 1c). SWNTs containing fullerenes (or peapods) come in bundles (Figure 1b), in which the fullerenes are encapsulated periodically in a 1D linear chain within the hollow core of the SWNT (Figure 1d). Subsequently, by thermally treating these peapods at 1700 °C in flowing argon using a graphite furnace, the growth of the inner tube from the coalescence of fullerenes and the formation of coaxial tubes were verified (Figure 1e) without any substantial change in the bundle structure. The reason for selecting 1700 °C is based on our previous study,[32] which showed that the photoluminescent signal was not observed in peapod-DWNTs that were thermally treated below 1600 °C, whereas a higher thermal treatment above 1700 °C resulted in bright PL and a strong absorption peak coming from the highly crystalline semiconducting inner tubes of peapod-DWNTs. However, incomplete filling of the newly formed inner tube was observed by TEM images (see short inner tubes in Supporting Information, Figure S2) due to the incomplete filling of fullerenes inside the tubes prior to the thermal treatment. An atomic TEM image of a CVD-DWNT also exhibits two coaxial tubes (Figure 1f). However, we were not able to find any significant difference between the TEM images of peapod- and CVD-DWNTs (compare Figure 1 panels e and f).

Since UV absorption constitutes a powerful tool to measure the metallicity and diameter distribution of SWNTs, homogeneously dispersed DWNT solutions were analyzed using an optical absorption spectrometer (Figure 2a).[34,35] The high-purity SWNT (diameter = 1.3−1.4 nm) suspension exhibits intense and sharp absorption peaks in the 900 and 1300 nm region coming from the second-order semiconducting transition (S_{22}), and a relatively weak absorption peak in the 500 and 800 nm range coming from the first-order metallic transition (M_{11}). However, the peapod-grown DWNT suspension shows distinctive features in the absorption spectrum. Specifically, the intensity of the M_{11} and S_{22} transitions of the outer tubes are largely depressed, whereas the newly appearing strong absorption peak around 1010 nm in the peapod-grown DWNT suspension is coming from the S_{11} transition of the semiconducting inner tubes. In contrast, the catalytically grown DWNT suspension has several strong absorption peaks in the range of 900−1300 nm.[36] For the DWNT suspensions, the absorption peaks in the region between 900 and 1300 nm are the result from the overlap of the S_{22} transition of the outer tube and the S_{11} transition for the inner tube. Theoretically, the intensity of the absorption peaks depends on the density of states of carbon nanotubes at the Fermi level, which is inversely proportional to the tube diameter. Therefore, the absorption peaks from the large diameter semiconducting outer tubes (>1 nm) are expected to be predominantly overlapped by the strong absorption peaks coming from the small-diameter (<1 nm) semiconducting inner tubes. This assumption is verified by the fact that the absorption spectra do not change before and after the photochemical treatment (Figure 2a). Our previous study revealed that the vacuum ultraviolet irradiation of Hipco-based SWNTs for 30 min introduced covalently anchored functional groups on the sidewalls of the nanotubes, resulting in the breakdown of the van Hove singularities (or the disappearance of the absorption peaks).[37] The above results indicate that both samples have a different diameter distribution as well as differences in metallicity, but the overlapped absorption peaks from the small-diameter inner tubes and the

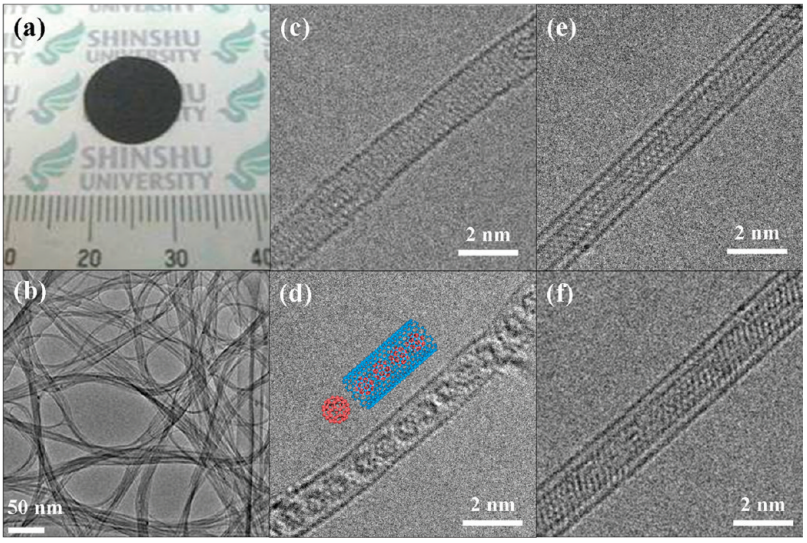

Figure 1. (a) A photograph of round (diameter = 3.4 cm) and black DWNT-derived bucky paper; (b) the low resolution TEM image exhibits intermingled bundles of DWNTs; (c) high resolution TEM images of the SWNT (hosting material), (d) SWNT encapsulating fullerenes periodically (also called peapods); (e) peapod-DWNT and (f) CVD-DWNTs. Note that peapod-DWNTs are prepared by thermally treating peapods at 1700 °C in an argon atmosphere using a graphite furnace, whereas CVD-DWNTs indicate the catalytically grown DWNTs. There is no any difference in the atomic resolution TEM images between the two kinds of DWNTs (e, f).

large-diameter outer tubes in the DWNTs, make it difficult for us to quantify the metallicity (or the chirality) of both types of tubes.

Thus, by carrying out a modified FFT image processing procedure,[38−41] we have identified the chirality of the inner and the outer tubes from the TEM images of the peapod- and CVD- DWNTs, as described in the Experimental Section and Supporting Information, Figure S1. TEM images of the DWNTs were fractioned into squares containing 2048 pixels (or 1024 pixels) per side. First, we used a Hamming window to eliminate the effect of the edges of square images. To achieve high resolution analysis, the spatial frequency analysis is carried out using a FFT on the enlarged image of the background. A chiral-type SWNT (chiral angle: $0° < \theta < 30°$) exhibits 12 spots (two 6 pairs on the front and the back), whereas only six spots are observed for armchair- and zigzag-type SWNTs. Thus, a DWNT exhibits 18 spots. Then, by separating the spots in three hexagons, we were able to obtain red-paired hexagons and a green single hexagon. As a result of the area-selected inverse FFT (IFFT), we obtained red-hexagons and green hexagons, corresponding to the inner tube and the outer tube, respectively. Eventually, we were also able to obtain the diameter and chiral angle of the inner and the outer tubes from the TEM images of the peapod- and CVD-DWNTs, and their corresponding FFT patterns, respectively (Figure 2b,c, Tables S1 and S2). We observed here smaller inner and outer diameters. We noted narrower chirality distributions for both the inner and the outer tubes as well as a smaller interlayer distance from the peapod-DWNTs as compared to that of the CVD-DWNTs. Such kinds of trends are strongly supported by measuring the two-dimensional photoluminescence maps of the peapod- and CVD-DWNT suspensions (Figure 2d,f). Each bright peak in the PL map corresponds to a specific (*n*,*m*) inner tube excited to the second excitonic transition S_{22}, and emitting a photon corresponding to its first excitonic transition S_{11}. It is very important to note that the PL map was confined to the small-sized tubes below 1.0 nm due to the limited ability of the detector used in these studies. However, we found that the chirality distributions of the small-sized tubes from the PL maps coming from both types of DWNTs are quite consistent with the data obtained from FFT image processing. In addition, the observed interlayer spacing for peapod-DWNTs with (6,5) inner tubes is consistent with the results obtained from the resonant Raman studies on isolated DWNTs.[42] According to the detailed chirality analysis, the metallic content of the inner and outer tubes for peapod-DWNTs was found to be 15% and 25%, whereas the corresponding values for the inner and the outer tubes of the CVD-DWNTs corresponded to 35% and 20%. The low metallic content in the inner tubes of the peapod-DWNTs could be explained by their special growth conditions, such as their high-temperature thermal treatment;[32] the fullerenes within the hollow core of SWNTs were coalesced to form corrugated tubes below 1700 °C, and these corrugated tubes were converted into energetically stable semiconducting and more crystalline tubes upon higher thermal treatments above 1700 °C.

Finally, we have examined the relationship between the metallicity of the inner and the outer tubes with measurement of the electric transport properties of peapod- and CVD-DWNT films. As shown in Figure 3, all nanotube films exhibit a semiconducting behavior.

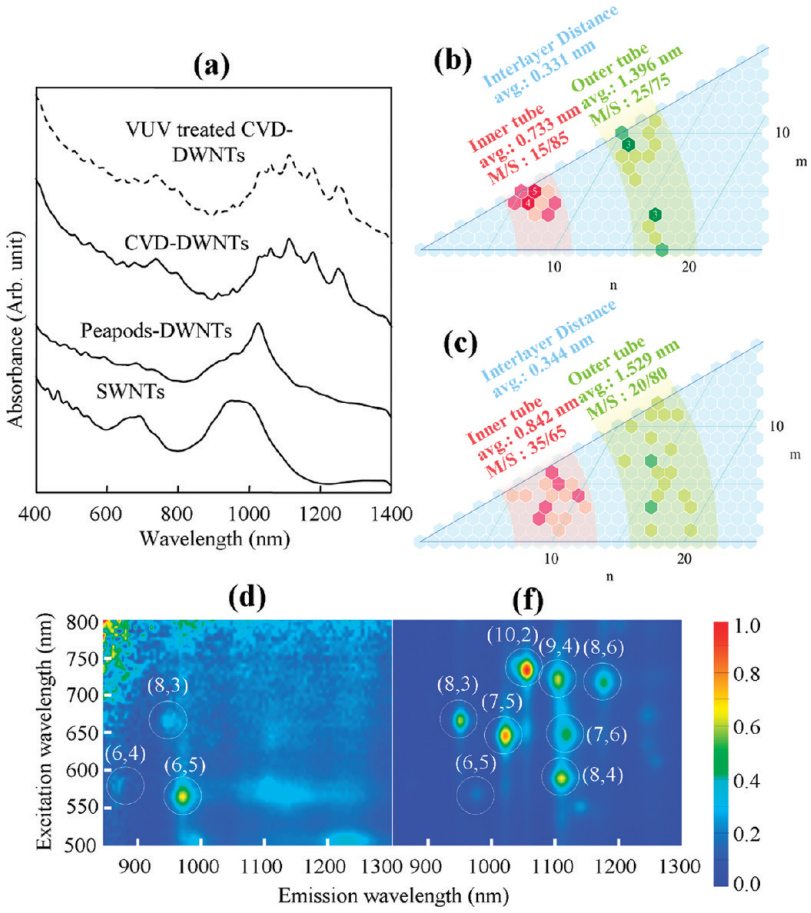

Figure 2. Metallicity evaluations of SWNTs, peapods- and CVD-DWNTs: (a) UV−vis absorption spectra of SWNTs, peapods- and CVD-grown DWNTs, and ultraviolet-treated CVD-grown DWNTs, (b, c) the chirality distribution of the inner and outer tubes of the peapod-DWNTs and the CVD-DWNTs are obtained *via* fast Fourier transform (FFT) image processing, and (d, f) two-dimensional photoluminescence maps of the peapods- and CVD-DWNT suspensions. Regarding the peapods-DWNTs that are synthesized by thermally treating peapods at 1700 °C in argon, the preferential growth of semiconducting (6,5) inner tubes was verified by a strong and sharp absorption peak at around 1010 nm (panel a), a bright photoluminescence signal (panel d) and the direct observation of 25% (6,5) tubes *via* a FFT imaging processing procedure (panel b).

By using the resistance ratio (ρ/ρ_{RT}), we are able to disregard the influence of the film thickness, density, and contact resistance. The lowest resistivity was found for films obtained from CVD-DWNTs. The resistivity was lower in CVD-DWNTs than in SWNT and peapod-DWNT films. We attribute this result to the total content of metallic tubes that the CVD-DWNT sample contains. No significant difference in the electrical resistivities of SWNT films and the peapod-DWNT films indicates the predominant role of the outer tubes in the transport. Thus, in order to understand (or study) the more obscure role of the inner tubes in the electrical transport, all samples were irradiated with ultraviolet radiation under vacuum for 30 min. The effectiveness of this photochemical reaction was confirmed by Raman spectroscopy (using a 633-nm laser line) on the SWNT film before and after vacuum-ultraviolet (VUV) treatment (Figure 4). The largely depressed radial breathing mode (RBM) around 160 cm^{-1}, the largely intensified D-band, and the disappearance of a Breit−-Wigner−Fano profile coming from the metallic tubes, indicate

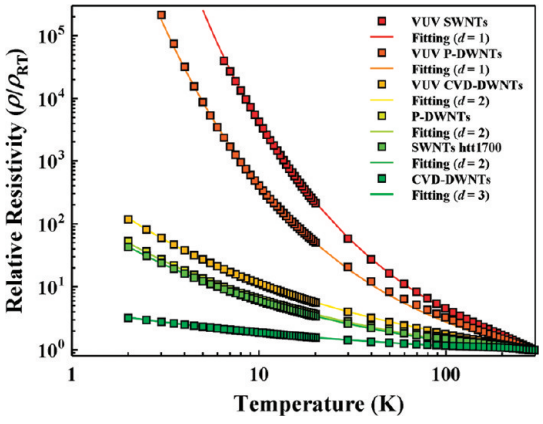

Figure 3. Temperature dependence of the normalized resistance of the SWNT, peapod-, and CVD-DWNT films before and after vacuum ultraviolet (VUV) treatment. The effectiveness of VUV treatment is verified by the largely increased resistance of all nanotube films.

the presence of covalently anchored functional groups on the sidewall of SWNTs,[37] thus resulting in a breakdown

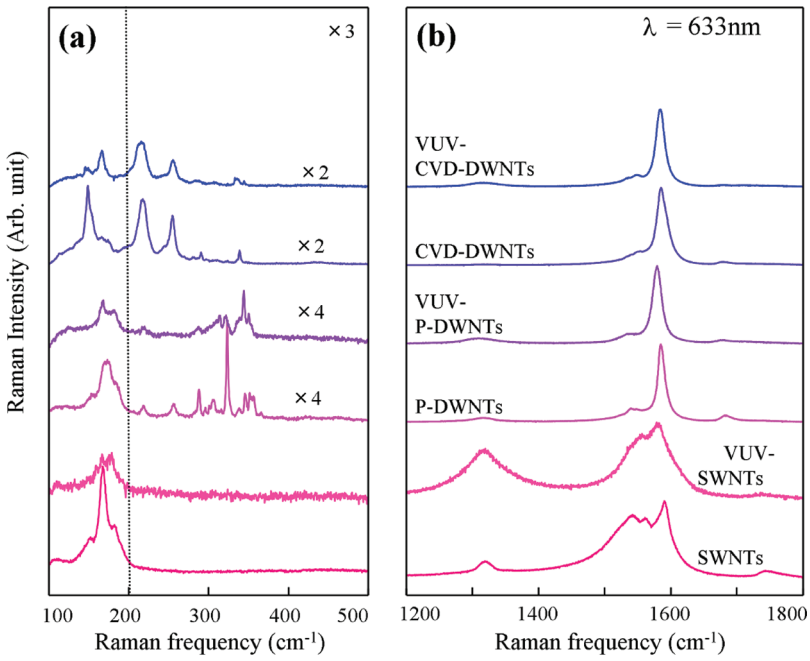

Figure 4. (a) Low- and (b) high-frequency Raman spectra of the SWNTs, peapod-, and CVD-DWNTs before and after vacuum ultraviolet treatment, using a 633 nm laser line.

of the sharpness of their van Hove singularities. From the low frequency Raman spectra of DWNT samples, we are able to assign two possible configurations (i.e., dominantly S@S and partially M@S). We could see a largely depressed radial breathing mode intensity of the outer tubes in VUV-treated DWNT samples. In addition, you can see a subtle change in the Raman frequency of the G band in the VUV-treated peapod-grown DWNT sample. In other words, the loss of the resonance condition for outer tubes can be the reason for the large depression of the G band and the RBM intensities. Thus, the strong G band as well as the absence of a D band in the VUV-treated DWNT samples is coming from the semiconducting inner tubes, because they are effectively protected from the oxidative chemical attack. Therefore, the large increase in the electric resistance of all VUV-treated nanotube films supports the effectiveness of the photochemical treatment. The covalent introduction of functional groups on the tube sidewalls leads to the disruption of the conjugated π bonding. If the electron transport of bulk CNTs depends only on their topological structure (*i.e.*, the number of layers and bulk structure), CVD- and peapod-DWNT films would show the same transport properties. However, we observed a large difference in the electric conductivity of peapod- and CVD-DWNT films. Among the many studies carried out on the electron transport in carbon nanotubes in the form of pellets and sheets,[43−45] the conduction mechanisms of SWNT networks have been well studied in terms of the fraction of their semiconducting (or metallic) nanotubes.[3] This study reported that the electron transport of the metallic SWNT film follows two-dimensional weak localization (2D-WL) theory, and with increasing content of semiconducting SWNTs, the conduction mechanisms are changed from 2D-WL, 3D-variable range hopping (VRH),[46] 2D-VRH[46] to 1D-VRH, consecutively.[47] 1D-VRH is sometimes called Coulomb-gap VRH. The resistivity ρ in VRH follows the following eq 1.

$$\rho(T) = \rho_0 \exp\left[\left(\frac{T_0}{T}\right)^{1/d+1}\right] \quad (1)$$

Here, d is the dimension of hopping, $d = 1$ for 1D-VRH (Efros−Shklovskii type) and $d = 2$ and 3 for 2D- and 3D-VRH (Mott type). T_0 is a characteristic temperature used in the VRH model. In our study, we used the dimension (d) as the indicator of the transport mechanism. The lines in Figure 3 are well fitted with VRH theory (see Figure S3). For VUV-treated nanotube films, we found the electrical resistivity to be in the order CVD-DWNTs < peapod-DWNTs < SWNTs. Even though peapod-DWNTs and SWNTs have almost a similar resistivity before the VUV treatment, the low resistivity observed in VUV-treated peapod-DWNT films when compared to SWNT films should be explained by the presence of the inner nanotube in DWNTs. This result provides strong experimental evidence showing that the inner nanotubes in DWNT films surely contribute to the observed electron transport behavior. Finally, the conduction mechanisms in SWNT, peapod- and CVD-DWNT films before and after VUV treatment are compared and summarized in Figure 5 as a function of the total content of their semiconducting nanotubes. The relative amount of the semiconducting tubes (the inner and outer tubes) is 55% for CVD-DWNTs, 40% for peapod-DWNTs, and 25% for SWNTs. Furthermore,

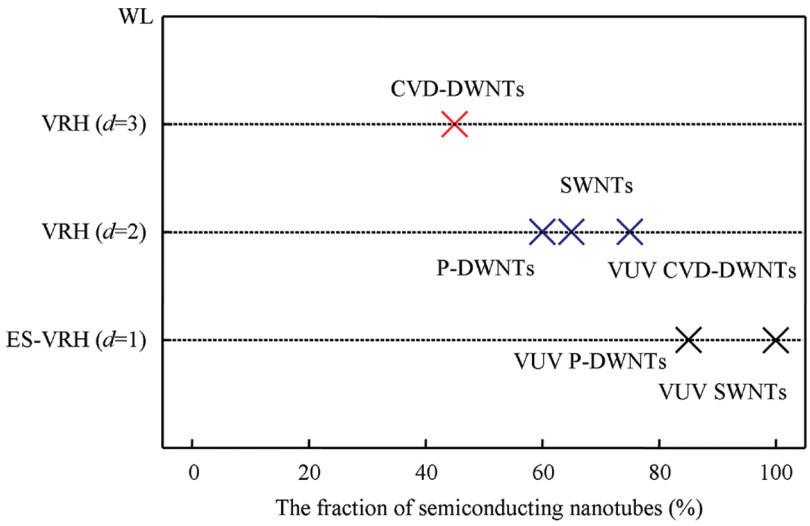

Figure 5. Variations of the conduction mechanisms in SWNT and DWNT films as a function of the relative content of the semiconducting inner and outer tubes (*d* value in VRH indicates conduction mechanisms, WL is weak localization, VRH is variable range hopping, ES-VRH indicates Coulomb gap VRH by the Efros & Shklovskii type).

assuming that all metallic outer nanotubes are modified by a VUV treatment, the content of semiconducting nanotubes in CVD-DWNTs, peapod-DWNTs and SWNTs is assumed to be 35%, 15%, and 0%, respectively. We found that the transport mechanisms are strongly dependent on the relative amount of metallic nanotubes contained in SWNT, peapod-, and CVD-DWNT films.

CONCLUSIONS

Herein, we have investigated the chirality-dependent conduction mechanisms in CVD- and peapod-DWNT films through identification of the chirality of the inner and the outer tubes using a FFT image processing method. The chirality distributions of the inner tubes in both types of DWNTs are closely consistent with the results from the PL maps of their corresponding DWNT suspensions. The low metallic content (*ca.* 15%) of the inner tubes of peapod-DWNTs, as compared with that of CVD-DWNTs (*ca.* 30%), is attributed to the fact that the inner tubes are grown from corrugated tubes *via* high temperature thermal treatment. The strong dependence of the transport mechanisms on the relative content of their metallic (or semiconducting) constituent nanotubes as well as the contribution of their inner nanotubes to electron transport in this work was confirmed by measuring the electrical conductivities of SWNTs, CVD-, and peapod-DWNTs before and after VUV treatment. The present work will be used as a model system for understanding the conduction mechanisms of MWNTs, and, furthermore, these findings will support the presently available theoretical background for the fabrication of high-performance transparent conductive films and filler material to be used in polymer composites.

EXPERIMENTAL SECTION

Synthesis of Catalytically and Peapod-Grown DWNTs. The high-purity and crystalline CVD-grown DWNTs were prepared as follows:[23] As-grown DWNTs were synthesized using a conditioning catalyst (Mo/Al_2O_3) at one end of the furnace, and a nanotube catalyst (Fe/MgO) in the middle part of the furnace. Subsequently, a methane and argon (1:1) mixture was fed into the reactor typically for 10 min at 875 °C. A purification process was applied to the as-grown products. First, an oxidation process (500 °C, 20 min) was carried out to reduce of the amount of chemically active SWNTs. Second a hydrochloric acid (18%, 100 °C, 10 h) treatment was carried out in order to remove magnesium oxide and iron catalysts, followed by air oxidation at 500 °C for 10 min in order to remove carbonaceous impurities. The detailed procedure of preparing peapod-grown DWNTs is as follows:[32] Highly purified arc-produced SWNTs (Hanwha Company, Korea) were used without further treatment. The SWNTs exhibit a diameter of about 1.3−1.4 nm and are used as the hosting fullerene material. After vaporizing fullerenes in a vacuum-sealed glass ampule containing SWNTs at 600 °C for 24 h, the reactants were washed twice in order to remove the residual fullerenes attached to the sidewall of the bundled SWNTs. Subsequently, the black paper-like peapods were dried under vacuum at 100 °C for 24 h. Finally, by subjecting the sample prepared *via* a high-temperature thermal treatment at 1700 °C in an argon atmosphere using a graphite furnace, high-purity peapod-derived DWNTs were obtained.

Photochemical Treatment. To clarify the contribution of the inner tube (or to disregard the influence of the outer tubes), DWNT films were subjected to a gas-phase photochemical treatment. A photochemical reaction was carried out by irradiating the prepared nanotube film with ultraviolet light from a xenon excimer lamp (UER172-200, Ushio Inc.) (λ = 172 nm) in air. The output power of the mercury lamp used in our study is 450 W. The power of the irradiated light was confined to 10 W/cm^2 by fixing the distance between the UV lamp and the sample at 30 mm.

Image Processing Procedure for Identifying the Chirality of the Inner and the Outer Tubes. Atomic resolution transmission electron microscopy (HR-TEM) images were obtained using double CS corrector (CEOS GmbH) equipped JEM-2100F (80 kV, JEOL, Japan). Then we selected a clean area of 5 nm square with no apparent tilt or focus difference of the nanotube and performed

the fast Fourier transform (FFT) to obtain the power spectrum of the selected area (Figure S1). The power spectrum nearly corresponds to the electron diffraction (ED) of the nanotube and therefore contains similar information, such as the angle of the hexagonal network arrangements of each layer (chiral angle), interlayer spacings, inclination (tilt) of the tube's longitudinal axis to the electron beam, and the diameter of each layer of the tube. Although the power spectrum contains rich information, it is hard to intuitively understand and reconstruct the image of each layer forming the nanotube. To obtain separate images of each layer, we need the information on the hexagonal network arrangement and the diameter. Obtaining the information on the hexagonal network arrangement is simple, because we only need to select six (10) spots rotationally separated by 60 degrees (yellow and green hexagons). The equatorial line is specified in order to obtain the composite information on the interlayer spacing and diameter of each layer. Therefore, it is cumbersome to obtain the information on the diameter of each tube from the equatorial line. To make things complicated, there are some variations of the interlayer spacings between the layers, and therefore the (002) spot becomes rather diffused. The easiest way to obtain the information on the tube diameter is to use the layer line that appears along the (10) spots (dotted lines). Since the layer line that originates from a certain (10) spot contains information on the diameter of the tube that made the particular (10) spot appear, the inverse FFT (IFFT) will recover the information on the diameter of that particular tube. The present method is convenient because we can simply make a mask that only includes the layer line and its corresponding (10) spots of the FFT image, and then perform the IFFT to reconstruct the hexagonal network image of each layer for the DWNTs.

Structural Characterizations. Raman spectra using a 633 nm-laser line were measured using a T64000 spectrometer (HORIBA Jobin Yvon Co.). To carry out optical studies for both DWNT samples, the nanotube sample was individually dispersed in heavy water with sodium dodecylbenzene sulfonate (0.5 wt %) under sonication for 1 h at 4 °C and subsequent ultracentrifugation (Optima Max-XP, Beckman Coulter, 322,100 g). The supernatants were carefully collected and used for subsequent optical studies with PL (Shimadzu, NIR-PL system) and an optical absorption spectrometer (Shimadzu, SolidSpec-3700). The measurement of the electrical conductivity of the DWNT films was carried out with a four probe method using a physical property measurement system (PPMS, Quantum Design Co.). The sample was cut into approximately 8 mm × 1 mm rectangles and the distance between the inner two leads is approximately 2 mm. We used a copper wire (diameter = 30 μm) as a lead and silver paste for contact between the copper wire and the surface of the DWNT film.

Acknowledgment. The authors acknowledge support from the Program for Fostering Regional Innovation in Nagano and a Grant-in-Aid (No. 19002007) from MEXT, Japan. M.S.D. acknowledges NSF1004147. M.T., Y.A.K., T.H., and M.E. acknowledge support from the Research Center for Exotic NanoCarbon Project, Japan regional Innovation Strategy Program by the Excellence, JST.

Supporting Information Available: Image processing procedure for identifying the chirality of the inner and the outer tubes (S1); typical TEM images of peapod-grown DWNTs (S2); tThe linearly fitted data using the VRH model with d = 3 (a), 2 (b−d), 1 (e, f) (S3); and the chirality distributions of the inner and the outer tubes in peapod-DWNTs (Table S1) and CVD-DWNTs (Table S2) using a FFT image processing procedure. This material is available free of charge *via* the Internet at http://pubs.acs.org.

REFERENCES AND NOTES

1. Baughman, R. H.; Zakhidov, A. A.; de Heer, W. A. Carbon Nanotubes-The Route Toward Applications. *Science* **2002**, *297*, 787–792.
2. Saito, R.; Fujita, M.; Dresselhaus, G.; Dresselhaus, M. S. Electronic Structure of Chiral Graphene Tubules. *Appl. Phys. Lett.* **1992**, *60*, 2204–2206.
3. Yanagi, K.; Kataura, H.; Udoguchi, H.; Ishida, T.; Sagitani, S.; Matsuda, K.; Oshima, Y.; Takenobu, T.; Maniwa, Y. Transport Mechanisms in Metallic and Semiconducting Single-Wall Carbon Nanotube Networks. *ACS Nano* **2010**, *4*, 4027–4032.
4. Pfeiffer, R.; Pichler, T.; Kim, Y. A.; , Kuzmany, H. Double-Walled Carbon Nanotubes. In *Carbon Nanotubes: Advanced Topics in the Synthesis, Structure, Properties and Applications*, Jorio, A., Dresselhaus, M. S., Dresselhaus, G., Eds.; Springer: New York, 2008, pp 495−530.
5. Hayashi, T.; Shimamoto, D.; Kim, Y. A.; Muramatsu, H.; Okino, F.; Touhara, H.; Shimada, T.; Miyauchi, Y.; Maruyama, S.; Terrones, M.; *et al.* Selective Optical Property Modification of Double-Walled Carbon Nanotubes by Fluorination. *ACS Nano* **2008**, *2*, 485–488.
6. Jung, Y. C.; Muramatsu, H.; Hayashi, T.; Kim, J. H.; Kim, Y. A.; Endo, M.; Dresselhaus, M. S. Covalent Attachment of Aromatic Diisocyanate to the Sidewall of Single- and Double-Walled Carbon Nanotubes. *Eur. J. Inorg. Chem.* **2010**, *27*, 4305–4308.
7. Brozena, A. H.; Moskowitz, J.; Shao, B. Y.; Deng, S. L.; Liao, H. W.; Gaskell, K. J.; Wang, Y. H. Outer Wall Selectively Oxidized, Water-Soluble Double-Walled Carbon Nanotubes. *J. Am. Chem. Soc.* **2010**, *132*, 3932–3938.
8. Shimada, T.; Sugai, T.; Ohno, Y.; Kishimoto, S.; Mizutani, T.; Yoshida, H.; Okazaki, T.; Shinohara, H. Double-Wall Carbon Nanotube Field-Effect Transistors: Ambipolar Transport Characteristics. *Appl. Phys. Lett.* **2004**, *84*, 2412–2414.
9. Yuan, S.; Zhang, Q.; Shimamoto, D.; Muramatsu, H.; Hayashi, T.; Kim, Y. A.; Endo, M. Hysteretic Transfer Characteristics of Double-Walled and Single-Walled Carbon Nanotube Field-Effect Transistors. *Appl. Phys. Lett.* **2007**, *91*, 143118.
10. Liu, K. H.; Wang, W. L.; Xu, Z.; Bai, X. D.; Wang, E. G.; Yao, Y. G.; Zhang, J.; Liu, Z. F. Chirality-Dependent Transport Properties of Double-Walled Nanotubes Measured *in Situ* on Their Field-Effect Transistors. *J. Am. Chem. Soc.* **2009**, *131*, 62–63.
11. Ha, B.; Shin, D. H.; Park, J.; Lee, C. J. Electronic Structure and Field Emission Properties of Double-Walled Carbon Nanotubes Synthesized by Hydrogen Arc Discharge. *J. Phys. Chem. C* **2009**, *112*, 430–435.
12. Kim, Y. A.; Kojima, M.; Muramatsu, H.; Umemoto, S.; Watanabe, T.; Yoshida, K.; Sato, K.; Ikeda, T.; Hayashi, T.; Endo, M.; *et al. In-Situ* Raman Study on Single- and Double-Walled Carbon Nanotubes as a Function of Lithium Insertion. *Small* **2006**, *2*, 667–676.
13. Kim, Y. A.; Muramatsu, H.; Park, K. C.; Shimamoto, D.; Jung, Y. C.; Kim, J. H.; Hayashi, T.; Saito, Y.; Endo, M.; Terrones, M.; *et al.* CdSe Quantum Dots-Decorated Double-Walled Carbon Nanotubes: The Effect of Chemical Moieties. *Appl. Phys. Lett.* **2008**, *93*, 051901.
14. Jung, Y. C.; Shimamoto, D.; Muramatsu, H.; Kim, Y. A.; Hayashi, T.; Terrones, M.; Endo, M. Conducting and Transparent Polymer Composites Using Surface-Modified and Individualized Double-Walled Carbon Nanotubes. *Adv. Mater.* **2008**, *20*, 4509–4512.
15. Neves, V.; Heister, E.; Costa, S.; Tilmaciu, C.; Borowiak-Palen, E.; Giusca, C. E.; Flahaut, E.; Soula, B.; Coley, H. M.; McFadden, J.; *et al.* Uptake and Release of Double-Walled Carbon Nanotubes by Mammalian Cells. *Adv. Funct. Mater.* **2010**, *20*, 3272–3279.
16. Green, A. A.; Hersam, M. C. Properties and Application of Double-Walled Carbon Nanotubes Sorted by Outer-Wall Electronic Type. *ACS Nano* **2011**, *5*, 1459–1467.
17. Green, A. A.; Hersam, M. C. Processing and Properties of Highly Enriched Double-Wall Carbon Nanotubes. *Nat. Nanotechnol.* **2009**, *4*, 64–70.
18. Hutchison, J. L.; Kiselev, N. A.; Krinichnaya, E. P.; Krestinin, A. V.; Loutfy, R. O.; Morawsky, A. P.; Muradyan, V. E.; Obraztsova, E. D.; Sloan, J.; Terekhov, S. V.; *et al.* Double-Walled Carbon Nanotubes Fabricated by a Hydrogen Arc Discharge Method. *Carbon* **2001**, *39*, 761–770.
19. Saito, Y.; Nakahira, T.; Uemura, S. Growth Conditions of Double-Walled Carbon Nanotubes in Arc Discharge. *J. Phys. Chem. B* **2003**, *107*, 931–934.

20. Huang, H.; Kajiura, H.; Tsutsui, S.; Murakami, Y.; Ata, M. High-Quality Double-Walled Carbon Nanotube Super Bundles Grown in a Hydrogen-Free Atmosphere. *J. Phys. Chem. B* **2003**, *107*, 8794–8798.
21. Li, X.; Li, F.; Liu, C.; Cheng, H. M. Synthesis and Characterization of Double-Walled Carbon Nanotubes from Multi-Walled Carbon Nanotubes by Hydrogen-Arc Discharge. *Carbon* **2005**, *43*, 623–629.
22. Sugai, T.; Yoshid, H.; Shimada, T.; Okazaki, T.; Shinohara, H. New Synthesis of High-Quality Double-Walled Carbon Nanotubes by High-Temperature Pulsed Arc Discharge. *Nano Lett.* **2003**, *3*, 769–773.
23. Endo, M.; Muramatsu, H.; Hayashi, T.; Kim, Y. A.; Terrones, M.; Dresselhaus, M. S. Buckypaper from Coaxial Structure. *Nature* **2005**, *433*, 476.
24. Kim, Y. A.; Muramatsu, H.; Hayashi, T.; Endo, M.; Terrones, M.; Dresselhaus, M. S. Fabrication of High Purity Double-Walled Carbon Nanotube Buckypaper. *Chem. Vap. Deposition* **2006**, *12*, 327–330.
25. Yamada, T.; Namai, T.; Hata, K.; Futaba, D. N.; Mizuno, K.; Fan, J.; Yudasaka, M.; Yumura, M.; Iijima, S. Size-Selective Growth of Double-Walled Carbon Nanotube Forests from Engineered Iron Catalysts. *Nat. Nanotechnol.* **2006**, *1*, 131–136.
26. Smith, B. W.; Monthioux, M.; Luzzi, D. E. Encapsulated C_{60} in Carbon Nanotubes. *Nature* **1998**, *396*, 323–324.
27. Smith, B. W.; Monthioux, M.; Luzzi, D. E. Carbon Nanotube Encapsulated Fullerenes: A Unique Class of Hybrid Materials. *Chem. Phys. Lett.* **1999**, *315*, 31–36.
28. Simon, F.; Kukovecz, Á.; Kramberger, C.; Pfeiffer, R.; Hasi, F.; Kuzmany, H.; Kataura, H. Diameter Selective Reaction Processes of Single-Wall Carbon Nanotubes. *Phys. Rev. B* **2005**, *71*, 165439.
29. Guan, L.; Shi, Z.; Li, M.; Gu, Z. Ferrocene-Filled Single-Walled Carbon Nanotubes. *Carbon* **2005**, *43*, 2780–2785.
30. Shiozawa, H.; Pichler, T.; Pfeiffer, R.; Kuzmany, H.; Kataura, H. Ferrocene Encapsulated in Single-Wall Carbon Nanotubes: A Precursor to Secondary Tubes. *Phys. Stat. Sol. (b)* **2007**, *244*, 4102–4105.
31. Bandow, S.; Takizawa, M.; Hirahara, K.; Yudasaka, M.; Iijima, S. Raman Scattering Study of Double-Wall Carbon Nanotubes Derived from the Chains of Fullerenes in Single-Wall Carbon Nanotubes. *Chem. Phys. Lett.* **2001**, *337*, 48–54.
32. Muramatsu, H.; Hayashi, T.; Kim, Y. A.; Shimamoto, D.; Endo, M.; Meunier, V.; Sumpter, B. G.; Terrones, M.; Dresselhaus, M. S. Bright Photoluminescence from the Inner Tubes of Peapod-Derived Double-Walled Carbon Nanotubes. *Small* **2009**, *5*, 2678–2682.
33. Muramatsu, H.; Hayashi, T.; Kim, Y. A.; Shimamoto, D.; Kim, Y. J.; Tantrakarn, K.; Endo, M.; Terrones, M.; Dresselhaus, M. S. Pore Structure and Oxidation Stability of Double-Walled Carbon Nanotube-Derived Bucky Paper. *Chem. Phys. Lett.* **2005**, *414*, 444–448.
34. Liu, X.; Pichler, T.; Knupfer, M.; Golden, M. S.; Fink, J.; Kataura, H.; Achiba, Y. Detailed Analysis of the Mean Diameter and Diameter Distribution of Single-Wall Carbon Nanotubes from Their Optical Response. *Phys Rev B* **2002**, *66*, 045411.
35. Jost, O.; Gorbunov, A. A.; Pompe, W.; Pichler, T.; Friedlein, R.; Knupfer, M.; Reibold, M.; Bauer, H.-D.; Dunsch, L.; Golden, M. S.; *et al.* Diameter Grouping in Bulk Samples of Single-Walled Carbon Nanotubes from Optical Absorption Spectroscopy. *Appl. Phys. Lett.* **1997**, *75*, 2217–2219.
36. Shimamoto, D.; Muramatsu, H.; Hayashi, T.; Kim, Y. A.; Endo, M.; Park, J. S.; Saito, R.; Terrones, M.; Dresselhaus, M. S. Strong and Stable Photoluminescence from the Semiconducting Inner Tubes within Double-Walled Carbon Nanotubes. *Appl. Phys. Lett.* **2009**, *94*, 083106.
37. Lee, S. H.; Jung, Y. C.; Kim, Y. A.; Muramatsu, H.; Teshima, K.; Oishi, S.; Endo, M. Optical Spectroscopic Studies of Photochemically Oxidized Single-Walled Carbon Nanotubes. *Nanotechnology* **2009**, *20*, 105708.
38. Zuo, J. M.; Vartanyants, I.; Gao, M.; Zhang, R.; Nagahara, L. A. Atomic Resolution Imaging of a Carbon Nanotube from Diffraction Intensities. *Science* **2003**, *300*, 1419–1421.
39. Gao, M.; Zuo, J. M.; Twesten, R. D.; Petrov, I. Structure Determination of Individual Single-Wall Carbon Nanotubes by Nanoarea Electron Diffraction. *Appl. Phys. Lett.* **2003**, *82*, 2703–2705.
40. Hirahara, K.; Kociak, M.; Bandow, S.; Nakahira, T.; Itoh, K.; Saito, Y.; Iijima, S. Chirality Correlation in Double-Wall Carbon Nanotubes as Studied by Electron Diffraction. *Phys. Rev. B* **2006**, *73*, 195420.
41. Giusca, C. E.; Tison, Y.; Stolojan, V.; Borowiak-Palen, E.; Silva, S. R. P. Inner-Tube Chirality Determination for Double-Walled Carbon Nanotubes by Scanning Tunneling Microscopy. *Nano Lett.* **2007**, *7*, 1232–1239.
42. Villalpando-Paez, F.; Muramatsu, H.; Kim, Y. A.; Endo, M.; Terrones, M.; Dresselhaus, M. S. Wall-to-Wall Stress Induced in (6,5) Semiconducting Nanotubes by Encapsulation in Metallic Outer Tubes of Different Diameters: A Resonance Raman Study of Individual C_{60}-Derived Double-Wall Carbon Nanotubes. *Nanoscale* **2010**, *2*, 406–411.
43. Skákalová, V.; Kaiser, A. B.; Woo, Y.-S.; Roth, S. Electronic Transport in Carbon Nanotubes: From Individual Nanotubes to Thin and Thick Networks. *Phys. Rev. B* **2006**, *74*, 085403.
44. Li, Z.; Kandel, H. R.; Dervishi, E.; Saini, V.; Biris, A. S.; Biris, A. R.; Lupu, D. Does the Wall Number of Carbon Nanotubes Matter as Conductive Transparent Material? *Appl. Phys. Lett.* **2007**, *91*, 053115.
45. Bandow, S.; Numao, S.; Iijima, S. Variable-Range Hopping Conduction in the Assembly of Boron-Doped Multiwalled Carbon Nanotubes. *J. Phys. Chem. C* **2007**, *111*, 11763–11766.
46. Mott, N. *Conduction in Non-Crystalline Materials*; Oxford University Press: Oxford, 1987.
47. Shklovskii, B. I.; Efros, A. L. *Electronic Properties of Doped Semiconductors*; Springer-Verlag: Berlin, 1984.